IEEE Access
Multidisciplinary | Rapid Review | Open Access Journal

Received January 5, 2021, accepted February 5, 2021, date of publication February 10, 2021, date of current version February 23, 2021.

Digital Object Identifier 10.1109/ACCESS.2021.3058412

A Distributed Dynamic Power Flow Algorithm for an Interconnected System Containing Two-Terminal LCC-HVDC Tie-Line

HAIBO ZHANG, (Senior Member, IEEE), AND SHUAI WANG

State Key Laboratory of Alternate Electrical Power System with Renewable Energy Sources, North China Electric Power University, Beijing 102206, China

Corresponding author: Haibo Zhang (zhb@ncepu.edu.cn)

This work was supported in part by the National Natural Science Foundation of China under Grant 51777069.

ABSTRACT In China, a growing number of regional power grids are interconnected by the line-commutated converter based high voltage direct current (LCC-HVDC) tie-line, forming a large-scale interconnected power grid. As the operation and control of the interconnected power grid are undertaken by multiple control centers, there is a demand for a distributed alternating current (AC)/direct current (DC) power flow algorithm. In this paper, a distributed power flow algorithm considering the LCC-HVDC tie-line is implemented based on the existing work of the author. The paper proposed some technologies to implement the algorithm. In the fixed-point iteration scheme of this paper, the combined boundary bus states are used to calculate the power flow of the DC system, thus the coordination of discrete state variables of the DC system is avoided. Also, the idea that converting the DC tie-line to an AC line is proposed to calculate the extended WARD equivalent of the external network of subsystems. Moreover, the unbalanced power distribution method is improved to make it more in line with the practical situation. Tests were carried out on the IEEE 118-bus system and an interconnected power grid constructed by six IEEE 118-bus systems, the correctness and effectiveness of the algorithm were proved.

INDEX TERMS Asynchronous iteration, distributed power flow, LCC-HVDC.

NOMENCLATURE

Constants:

N	Number of buses of the whole system.
N_S	Number of subsystems of the whole system.
N_{DI}	Number of subsystems in the DI region.

Variables:

U_{dR}, U_{dI}	DC voltage of rectifier side and inverter side.
U_{d0R}, U_{d0I}	No-load DC voltage of rectifier side and inverter side.
δ_R, δ_I	Control angle of rectifier and inverter.
ϕ_R, ϕ_I	Power factor angle of rectifier side and inverter side.
X_{dR}, X_{dI}	Commutation reactance of rectifier side and inverter side.
$P_{DC.R}$, $P_{DC.I}$	Active power injection at PCC bus of rectifier side and inverter side.
$Q_{DC.R}$, $Q_{DC.I}$	Reactive power injection at PCC bus of rectifier side and inverter side.
T_R, T_I	Turns ratio of converter transformer of rectifier side and inverter side.
$\dot{U}_R$, $\dot{U}_I$	PCC voltage of rectifier side and inverter side. The voltage phase angle is θ_R and θ_I.
θ_{RI}	Phase angle difference $\theta_R - \theta_I$.
I_d	DC current.
R_d	Resistance of DC transmission line.
B	Number of converter bridge.
$\dot{S}_{DC}$	Power injection into the DC system.
$\dot{U}_{PCC}$	PCC voltage.
T	Turns ratio of converter transformer.
C	Control mode of the DC system.
T', C'	Turns ratio and control mode obtained from the power flow calculation of the DC system.
$f_{DC}(\cdot)$	A mapping that represents the power flow calculation of the DC system.

The associate editor coordinating the review of this manuscript and approving it for publication was S. Srivastava.

ΔP_i	Power mismatch of bus i.
P_{Gi0}	Generator's initial active power injection at bus i.
P_{Di}	Active power of the load at bus i.
$P_{DC.i}$	Active power consumption of DC system at bus i.
U_i	Voltage magnitude of bus i.
G_{ij}, B_{ij}	Conductance and susceptance elements at row i and column j of the bus admittance matrix.
β_i	Distribution coefficients of bus i.
P_{acc}	Unbalanced power when the AC PF calculation converges.
ΔP_{acc}	Error of unbalanced power in the AC PF iteration.
$\dot{S}_i^{eq}$	Equivalent power injection into external boundary bus i.
$\hat{\mathbf{x}}_B^{(l)}$	Combined boundary bus states in l-th outer iteration step.
$f_{BE(k)}(\cdot)$	A mapping between equivalent power injection into external boundary buses and boundary bus states of the subsystem k.
$\phi_{(k)}(\cdot)$	A mapping between equivalent power injection, power injection into the DC system, and boundary bus states of subsystem k.
$\dot{\mathbf{x}}_{B(k)}^{(l+1)}$	Boundary bus states that are calculated by subsystem k in the $(l+1)$-th outer iteration.
ξ_k	Combination parameters of subsystem k.
$T_{(k)}^{(l+1)}$, $C_{(k)}^{(l+1)}$	Turns ratio of converter transformer and control mode calculated by subsystem k.
$\hat{T}^{(l+1)}$, $\hat{C}^{(l+1)}$	Turns ratio of converter transformer and control mode after combination calculation.
$\varphi_{(k)}$	$\varphi_{(k)}$ represents the AC/DC power flow calculation which adopts the sequential method.
η_k	Combination parameters of discrete variables T and C.
$\dot{S}_{DC(k)}^{(l+1)}$	Power injection into the DC system calculated by subsystem k.
G_{DC}^{eq}, B_{DC}^{eq}	Branch conductance and susceptance of the equivalent AC transmission line.
$b_{DC.R}^{eq}$, $b_{DC.I}^{eq}$	Shunt susceptance of equivalent AC transmission line.
ΔP_{SYSj}	Unbalanced power of subsystem j.
β_{SYSj}	Sum of the distribution coefficients of all buses in subsystem k (excluding external boundary buses).
$\Delta\tilde{P}_{SYSj}$	Unbalanced power that should be taken by subsystem j.
$\Delta P'_{BE.SYSj}$	Difference between ΔP_{SYSj} and $\Delta\tilde{P}_{SYSj}$.
$P_{BE.i}^{\prime(l)}$	Revised equivalent power injection at bus i in the l-th outer iteration.
$\mu_{BE.i}$	External network equivalent of injection variation coefficients of bus i.

I. INTRODUCTION

The simultaneous calculation executed in the integrated network model in existing energy management systems (EMSs) may present challenges when the concerned network consists of different types of systems operated by different entities (independent system operators, transmission system operators, or utilities). Based on the background of the construction of a distributed energy management system (DEMS) in the market environment, reference [1] proposed a distributed dynamic power flow algorithm with multiple control centers applicable to the alternating current (AC) system. In the DEMS system designed in [1], the application closely related to the detailed equipment model, such as state estimation and dispatcher power flow, was realized in the way of decomposition and coordination calculation. The detailed equipment models were maintained by each control center, and graphics platforms could be shared through the web or scalable vector graphics (SVG) if allowed by the market environment, so other advanced applications of local EMS can perform an accurate calculation based on the whole network bus model obtained from the distributed power flow calculation of [1].

Existing studies on distributed computation mainly involve distributed power flow calculation [1], [2], distributed optimal power flow [3]–[5], and distributed state estimation [6], [7]. For distributed power flow calculation, it needs to be distinguished from parallel power flow calculation [8], [9]. The parallel calculation aims at improving the computation speed and is carried out in the computing cluster in which the communication between computers is very reliable. However, in the distributed calculation, the computers in each control center are far away geographically, so communication is an important factor to be considered. A distributed optimal power flow problem can be solved by different distributed optimization technologies, such as the auxiliary problem principle [3], the alternating-direction method of multipliers (ADMM) [4], and the augmented Lagrangian alternating-direction inexact Newton method [5]. Reference [4] chose to split the network at the boundary buses, took the equality of boundary bus states of different subsystems as the constraint, and solved the optimal power flow through ADMM. Like the distributed optimal power flow, the distributed state estimation can also be solved by the distributed optimization techniques, such as constructing an alternative solution mode based on the Lagrange multiplier method [6] or using ADMM to solve the state estimation problem [7]. The convergence of this category of algorithms is not very ideal.

Since the AC system and the direct current (DC) system are naturally decoupled at the point of common coupling, the distributed power flow calculation can be realized by calculating

the AC system and the DC system alternately [10]. Reference [11] decomposed the whole estimation problem into an AC and a DC state estimation problem to realize the distributed state estimation. Also, the Lagrange relaxation method was usually adopted to decouple the constraints between the AC and the DC systems [12], [13]. Similarly, the optimal operation scheduling problem of the AC/DC system was divided into the AC subproblem and the DC subproblem, and the global optimal solution was obtained by solving the AC subproblem and DC subproblem alternately [14]. In addition, an AC/DC decoupling model was established in [15], which is composed of a converter station, a DC distribution network, and an AC distribution network. Reference [16] considered the situation of AC/DC hybrid tie-lines and selected the voltage of AC and DC tie-line as boundary bus states to ensure the same power flow of tie-line obtained by different subsystems. Most of the above references are based on the voltage-sourced converter based high voltage direct current (VSC-HVDC) system and only studies the situation of pure DC tie-line.

Compared with the VSC-HVDC system, the line-commutated converter (LCC) based HVDC system contains discrete state variables that are difficult to be coordinated in the distributed calculation. Therefore, it is more difficult to implement a distributed power flow algorithm considering the LCC-HVDC tie-line. Moreover, LCC-HVDC is widely used in practical projects, and more than 30 LCC-HVDC projects have been put into operation in China. Therefore, there is a practical demand for the distributed power flow algorithm considering the LCC-HVDC tie-line.

In this paper, the distributed AC/DC power flow algorithm is implemented based on [1], i.e., the present paper is a continuation of that research effort. The main work of this paper is as follows:

1) Improve [1] to realize the distributed AC/DC power flow algorithm. Although the current centralized AC/DC power flow algorithm is mature [17], [18], how to effectively combine it with the algorithm of [1] still faces many challenges. One of the difficulties is that the LCC-HVDC system contains discrete state variables that are inconvenient to be coordinated in the distributed calculation. In this paper, the reasonable design makes the distributed computing achieve reliable convergence and get correct results without coordinating the discrete state variables. The contents of this part: Modeling and power flow calculation method of AC/DC system (Section II), modeling method of the subsystem (Section III), construction of fixed-point iteration scheme (Section IV, part A and B).

2) The unbalanced power distribution method in [1] is improved to make it more in line with the actual situation (Section IV, part C).

II. THE SEQUENTIAL METHOD OF THE AC/DC POWER FLOW CALCULATION

The AC/DC power flow algorithm can be divided into two categories: the unified method [17] and the sequential method [18]. This paper adopts the sequential method to calculate the AC/DC power flow. According to the sequential algorithm, the AC system and the DC system calculate the power flow alternately and exchange the boundary variables until the exchange variables no longer change.

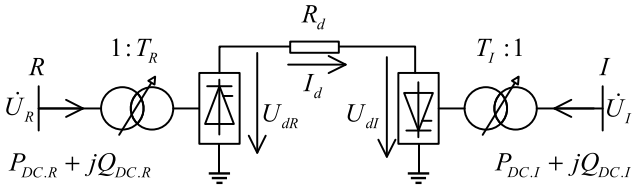

FIGURE 1. Schematic diagram of the two-terminal LCC-HVDC system.

A. THE MODEL AND POWER FLOW CALCULATION OF TWO-TERMINAL LCC-HVDC SYSTEM

A diagrammatic sketch of the two-terminal LCC-HVDC system is shown in Fig. 1. The DC system consists of two converters, a DC line, and two converter transformers (T_R and T_I are the turns ratio). The connection points between the AC system and DC system are called the point of common coupling (PCC), namely bus R and bus I. According to the reference direction of power flow, $P_{DC.R}+jQ_{DC.R}$ and $P_{DC.I}+jQ_{DC.I}$ are defined as the power injection into the DC system (PIDC)

The converter adopts the quasi-steady-state model [19] in the power flow calculation of the DC system (DC PF), and the corresponding equation of the converter is shown in (1).

$$\begin{cases} U_{d0R} &= \dfrac{3\sqrt{2}}{\pi} B T_R \left|\dot{U}_R\right| \\ U_{dR} &= U_{d0R}\cos\delta_R - \dfrac{3}{\pi} X_{dR} I_d B \\ \phi_R &= \cos^{-1}\left(U_{dR}/U_{d0R}\right) \\ Q_{DC.R} &= P_{DC.R}\tan\phi_R \\ P_{DC.R} &= U_{dR} I_d \end{cases} \tag{1}$$

The corresponding equation of the DC line is shown in (2).

$$U_{dR} - U_{dI} = I_d R_d \tag{2}$$

The PCC voltage, the converter transformation ratio, and the control mode of the converter are defined as the state variables of the DC system. According to (1) and (2), Once these state variables are determined, the operation state of the DC system can be completely determined. Also, the DC system can adjust the converter transformer's tap changer and the control mode according to its operation states. Therefore, the DC PF can be expressed by the following functional relations.

$$\left\{\dot{S}_{DC}, T', C'\right\} = f_{DC}\left(\dot{U}_{PCC}, T, C\right) \tag{3}$$

In the above equation, $\dot{U}_{PCC}$ is obtained from the AC PF, and $\dot{S}_{DC}$ will be sent to the AC system to perform the AC PF.

B. THE POWER FLOW CALCULATION OF THE AC SYSTEM

The dynamic power flow algorithm proposed in [20], [21] is adopted to calculate the power flow of the AC system (AC PF). This dynamic power flow algorithm distributes the

unbalanced power P_{acc} of the whole network caused by a disturbance in all generator buses according to the distribution factor β_i of generator buses, thus canceling the concept of the slack bus and making the power flow calculation results more consistent with reality. Assuming that there are N buses in a system and bus 1 is the reference bus, then N-1 active power mismatch equations can be listed. The active power mismatch equation of bus i is shown as (4). According to the sequential method, the DC system is regarded as a load at PCC in the AC PF.

$$\begin{aligned}\Delta P_i = {} & P_{Gi0} - P_{Di} - P_{DC.i} \\ & - U_i \sum_{j \in i} U_j \left(G_{ij} \cos\theta_{ij} + B_{ij} \sin\theta_{ij}\right) \\ & - \beta_i P_{acc} \quad (i = 2, \cdots N)\end{aligned} \tag{4}$$

When the system returns to the steady-state of the same frequency after the disturbance, the unbalanced power P_{acc} of the whole network is the difference between the initial output of all generators in the system and the actual power consumption (the sum of the actual load and the actual transmission loss). P_{acc} is unknown before the power flow calculation, so an unknown variable is added in (4) and an equation should be added at the reference bus 1 where both U_1 and θ_1 are known, which is shown in (5).

$$\begin{aligned}\Delta P_1 = {} & P_{G10} - P_{D1} \\ & - U_1 \sum_{j \in 1} U_j \left(G_{1j} \cos\theta_{1j} + B_{1j} \sin\theta_{1j}\right) - \beta_1 P_{acc}\end{aligned} \tag{5}$$

Assuming that the number of PQ buses of the system is ND. When ND equations of reactive power mismatch are added, the above equation set can be solved by referring to the fast-decoupled power flow algorithm [22]. The reactive power iteration scheme is not different from the conventional power flow algorithm, while in the correction formula of the active power iteration part, the correction formula of the new variable P_{acc} needs to be added, as shown in (6)

$$\Delta P_{acc} = -\sum_{i=1}^{N} \frac{\Delta P_i}{U_i} \Bigg/ \sum_{i=1}^{N} \frac{\beta_i}{U_i} \tag{6}$$

The final P_{acc} is obtained when the dynamic power flow converges. For more details of dynamic power flow, please refer to [20], [21], which will not be repeated here.

III. THE MODEL OF DISTRIBUTED POWER FLOW CALCULATION

A. THE CALCULATION MODEL OF SUBSYSTEM

The subsystem model consists of the internal network, tie-line, and external network equivalent. The external network equivalent model of the subsystem is calculated according to the extended WARD equivalent method [23]. The extended WARD equivalent method is a WARD-type equivalent method, which is applicable to model the external network in EMS. Compared with the classic WARD equivalent, the extended WARD equivalent can more accurately simulate the reactive power response of the external network to the state change of the internal network. Therefore, the extended WARD equivalent is suitable for the independent calculation of subsystems and can improve the convergence of the distributed calculation.

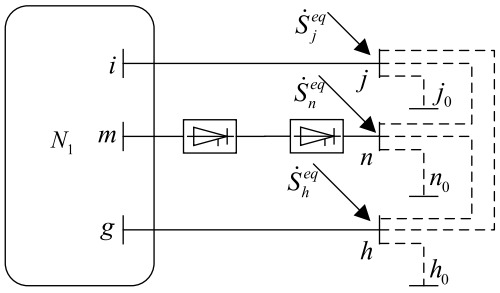

FIGURE 2. The model of the subsystem.

Fig. 2 shows a schematic diagram of the subsystem modeling. In this figure, N_1 is the detailed model of the internal network, and branch ij, mn, and gh are the tie-line. The external network equivalent model on the right side includes the equivalent branches between the boundary buses, the equivalent power injection at the boundary buses ($\dot{S}_j^{eq}$, $\dot{S}_n^{eq}$, and $\dot{S}_h^{eq}$), and the fictitious PV buses connected at the boundary buses (j_0, n_0, and h_0).

Since there are DC tie-lines in the external network of the subsystem, special treatment is needed for the DC tie-lines in the extended WARD equivalent, which will be introduced later in Part B

B. THE EQUIVALENT OF THE LCC-HVDC SYSTEM

It involves the network equivalent of the AC/DC system when the coordinator calculates the exterior network equivalent model of each subsystem and the combination parameters of the boundary buses. Since it is difficult to deal with LCC-HVDC lines in network equivalent, this paper converts the DC line into an AC line when calculating the external network equivalent model.

The parameters of the equivalent AC line are not related to the internal characteristics of the DC system but are related to the voltage and power injection at both terminals of the DC system. The equivalent AC transmission line is shown in Fig. 3.

The admittance $G_{DC}^{eq} + jB_{DC}^{eq}$, the susceptance $b_{DC.R}^{eq}$ and $b_{DC.I}^{eq}$ are the unknown variables to be determined, the calculation formula is shown in (7).

$$\begin{cases} G_{DC}^{eq} = \dfrac{P_{DC.R} + P_{DC.I}}{U_R^2 + U_I^2 - 2U_R U_I \cos\theta_{RI}} \\ B_{DC}^{eq} = \dfrac{\left(U_R^2 - U_I^2\right) G_{DC}^{eq} - \left(P_{DC.R} - P_{DC.I}\right)}{2U_R U_I \sin\theta_{RI}} \\ b_{DC.R}^{eq} = \left[-Q_{DC.R} + \left(U_R U_I \cos\theta_{RI} - U_R^2\right) B_{DC}^{eq} \right. \\ \left. - U_R U_I G_{DC}^{eq} \sin\theta_{RI}\right] \Big/ U_R^2 \\ b_{DC.I}^{eq} = \left[-Q_{DC.I} + \left(U_R U_I \cos\theta_{RI} - U_I^2\right) B_{DC}^{eq} \right. \\ \left. + U_R U_I G_{DC}^{eq} \sin\theta_{RI}\right] \Big/ U_I^2 \end{cases} \tag{7}$$

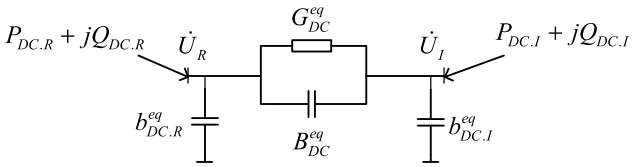

FIGURE 3. Schematic diagram of the equivalent AC transmission line.

In this paper, there are two modeling methods for the DC system. One is the quasi-steady-state model mentioned in section II, which is used to calculate the DC PF. The other is the equivalent AC line model here, this model is only used to calculate the external network equivalent parameters of each subsystem and the combination parameters.

IV. IMPLEMENTATION DETAILS OF DISTRIBUTED POWER FLOW ALGORITHM

A. THE FIXED-POINT ITERATIVE SCHEME DERIVED FROM THE SIMPLE EXTENSION OF [1]

The core content of [1] and this paper is the construction of the fixed-point iterative scheme. The fixed-point iteration scheme in [1] is as follows:

$$\begin{cases} \left\{\dot{\mathbf{x}}_{B(k)}^{(l+1)}\right\} = \phi_{(k)}\left(f_{BE(k)}(\hat{\mathbf{x}}_B^{(l)})\right) \\ \hat{\mathbf{x}}_B^{(l+1)} = \sum_{k=1}^{N_S} \xi_k \cdot \dot{\mathbf{x}}_{B(k)}^{(l+1)} \end{cases} \tag{8}$$

The first equation in (8) represents the independent dynamic power flow calculation of the subsystem, and the second equation represents the combination calculation of the subsystem, these two formulas construct a fixed-point iteration step. As the AC PF of the subsystem also needs the iterative calculation, the fixed-point iteration is defined as the outer iteration, and the AC PF of the subsystem is defined as the inner iteration.

A simple way to realize the distributed AC/DC power flow algorithm is to replace the inner iteration of (8) with the AC/DC power flow calculation. In addition, as the DC tie-line contains additional discrete state variables compared with the AC tie-line, it is necessary to combine not only the boundary bus states of all tie-lines but also the discrete state variables of the DC tie-line. The fixed-point iteration scheme is shown in (9):

$$\begin{cases} \hat{\mathbf{x}}_B^{(l)} = \sum_{k=1}^{N_S} \xi_k \cdot \dot{\mathbf{x}}_{B(k)}^{(l)} & (9.1) \\ \left\{\hat{T}^{(l)}, \hat{C}^{(l)}\right\} = \sum_{k=1}^{N_S} \eta_k \cdot \left\{T_{(k)}^{(l)}, C_{(k)}^{(l)}\right\} & (9.2) \\ \left\{\dot{\mathbf{x}}_{B(k)}^{(l+1)}, T_{(k)}^{(l+1)}, C_{(k)}^{(l+1)}\right\} = \varphi_{(k)}\left(f_{BE(k)}(\hat{\mathbf{x}}_B^{(l)}), \hat{T}^{(l)}, \hat{C}^{(l)}\right) & (9.3) \end{cases}$$

In the above equation, (9.1) represents the combination calculation of boundary bus states. (9.2) represents the combination calculation of the discrete state variables, and it should be noted that the combination calculation of the discrete state variables is not simple addition, but for the sake of formal simplicity, the combination calculation of the discrete state variables is represented in the form of weighted addition. (9.3) represents the AC/DC power flow calculation of the subsystem.

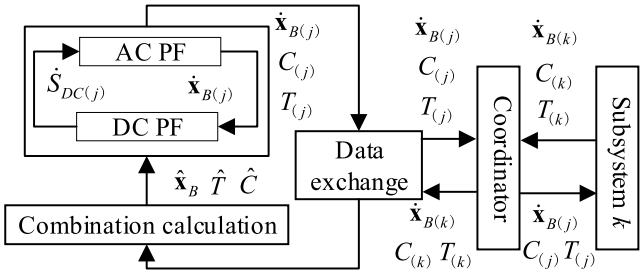

FIGURE 4. A brief flow chart of the algorithm in part A.

The calculation process starts with the AC/DC power flow, and the initial value of iteration, i.e., $\hat{\mathbf{x}}_B^{(0)}$, $\hat{T}^{(0)}$, $\hat{C}^{(0)}$, is obtained from the base states.

A brief flowchart for this fixed-point iteration scheme is shown in Fig. 4. According to (9), the AC PF and DC PF have performed alternately till the AC/DC power flow converges, then the outer iteration steps are performed.

Because of the disturbance, the power flow results of the subsystem in the early stage are quite different from the correct results, which may lead to the inaccurate adjustment of the converter transformer's tap changer. Compared with continuous variables, the discrete state variables' combination calculation causes some loss of calculation accuracy, which may lead to the situation that the converter transformer's tap position or the control mode of each subsystem is inconsistent. Therefore, the effect of this distributed calculation mode is not very ideal.

B. THE FIXED-POINT ITERATIVE SCHEME OF THIS PAPER RECOMMENDED

The model of the DC system is the same in each subsystem, and the adjustment results of the converter transformer's tap changer and control mode are only related to the previous calculation results of the DC system. If the initial converter transformer's tap position and control mode of each subsystem are the same and each subsystem makes use of the same boundary bus states to do the DC PF, the consistent power flow results of the DC system can be ensured.

Based on the above ideas, subsystems perform the combination calculation of boundary bus states before performing the DC PF. In addition, only one AC PF and one DC PF are performed in one outer iteration. The process of the fixed-point iteration scheme is shown in (10).

$$\begin{cases} \hat{\mathbf{x}}_B^{(l)} = \sum_{k=1}^{N_S} \xi_k \cdot \dot{\mathbf{x}}_{B(k)}^{(l)} & (10.1) \\ \left\{\dot{S}_{DC(k)}^{(l)}, T_{(k)}^{(l+1)}, C_{(k)}^{(l+1)}\right\} = f_{DC}\left(\hat{\mathbf{x}}_B^{(l)}, T_{(k)}^{(l)}, C_{(k)}^{(l)}\right) & (10.2) \\ \dot{\mathbf{x}}_{B(k)}^{(l+1)} = \phi_{(k)}\left(f_{BE(k)}(\hat{\mathbf{x}}_B^{(l)}), \dot{S}_{DC(k)}^{(l)}\right) & (10.3) \end{cases}$$

In the above equation, (10.1) represents the combination calculation, (10.2) represents the DC PF calculation, and (10.3) represents the AC PF calculation.

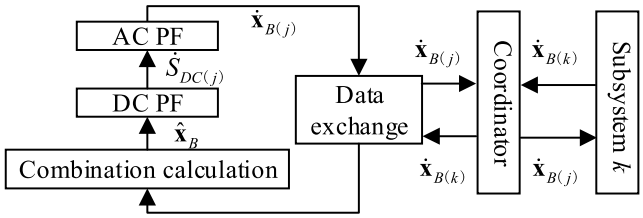

FIGURE 5. A brief flow chart of the algorithm in part B.

The calculation process starts with the DC PF, and the initial value of iteration is obtained from the base states. The brief flow chart corresponding to (10) is shown in Fig. 5. The state variables of the DC systems of different subsystems are the same in each DC PF, so the calculation results will be the same and it is not necessary to perform the combination calculation for the discrete state variables.

The subsystem only performs one DC PF and one AC PF in an outer iteration step, which is different from part A. The AC/DC power flow calculation of the subsystem gradually converges with the outer iteration progressing, which also belongs to the calculation mode of the sequential method described in Section II.

C. THE DISTRIBUTION OF UNBALANCED POWER

The distribution method of unbalanced power in [1], which distributes the unbalanced power to all generator buses, is not quite in line with the actual situation and is improved in this paper.

In the algorithm of [1], the unbalanced power caused by disturbance will be compensated by all generators in the whole system, so all subsystems participate in the unbalanced power distribution. However, the actual situation is different. When a disturbance occurs in the interconnected system, the subsystem in which the disturbance occurs will conduct system frequency regulation to balance the unbalanced power while neighboring subsystems provide power support. The remaining subsystems generally follow the control requirements of the secondary frequency regulation (assumed to be TBC control mode) to keep the power flow of the tie-line constant. The unbalanced power in these subsystems is the variation of transmission loss, which is a small value.

It can be seen that the influence caused by the disturbance is limited to the subsystem with disturbance and its neighboring subsystem, rather than spread to the whole system. Therefore, the concept of disturbance influence region is introduced here, and the internal region and external region of disturbance influence are defined, namely the DI region and the DE region. According to the definition, the subsystem with disturbance and its neighboring subsystems are located in the DI region, and the remaining subsystems are located in the DE region

The reasonable distribution of the unbalanced power among subsystems is realized by correcting the power injection into external boundary buses. This method is applied to the distribution of the unbalanced power among the subsystems in the DI region in this paper, which is briefly introduced below.

Suppose that the unbalanced power P_{acc} calculated by subsystem k in the DI region is ΔP_{SYSk}, and the unbalanced power that should be taken by subsystem j as $\Delta\tilde{P}_{SYSj}$. The calculation formula of $\Delta\tilde{P}_{SYSj}$ is shown in (11):

$$\Delta\tilde{P}_{SYSj} = \frac{\beta_{SYSj}}{\sum_{k=1}^{N_{DI}} \beta_{SYSk}} \cdot \sum_{k=1}^{N_{DI}} \Delta P_{SYSk} \tag{11}$$

The unbalanced power difference $\Delta P'_{BE.SYSj}$ between the actual unbalanced power and the unbalanced power of each subsystem that should be taken is calculated by (12).

$$\Delta P'_{BE.SYSj} = \Delta\tilde{P}_{SYSj} - \Delta P_{SYSj} \tag{12}$$

Every external boundary bus in subsystem j will undertake a portion of the unbalanced power difference $\Delta P'_{BE.SYSj}$, as shown in (13).

$$P'^{(l)}_{BE.i} = P^{(l)}_{BE.i} + \mu_{BE.i} \cdot \Delta P'^{(l)}_{BE.SYSj} \tag{13}$$

It should be pointed out that in the equivalent calculation of the injection variation coefficients (it is shown in (23) and (24) in [1]), all DC tie-lines involved should be replaced by the equivalent AC transmission lines of the DC system, and the distribution coefficient of each bus in the DE region needs to be treated as zero.

V. FLOW CHART OF THE ALGORITHM

Fig. 6 shows the flow chart of the algorithm, in which the different part between this algorithm and the algorithm of [1] is marked as light blue. The algorithm process is divided into three stages, namely real-time equivalent stage, initialization of asynchronous iteration stage, and asynchronous iteration stage.

1) Real-time equivalent. Each subsystem builds its local model and calculates the internal network equivalent parameters and the internal equivalent coefficients. The coordinator calculates the equivalent AC transmission line according to (10) and the external network equivalent parameters which will be sent to each subsystem. Besides, the external network equivalent of injection variation coefficients $\mu_{BE.i}$ is calculated and sent to subsystems. $\mu_{BE.i}$ is related to the distribution of unbalanced power (refer to (13)).
2) Initialization of asynchronous iteration. The subsystem calculates the diagonal elements of the boundary bus impedance matrix excluding external equivalent branches. Then, the coordinator forwards the information to each subsystem. After receiving the information, the subsystem calculates the combination parameters.
3) Asynchronous iteration. The coordinator sends the boundary bus states, unbalanced power (if the subsystem is located in the DI region), and the convergence flag of one subsystem to other relevant subsystems. After receiving the information from the coordinator, the subsystem calculates the combined boundary

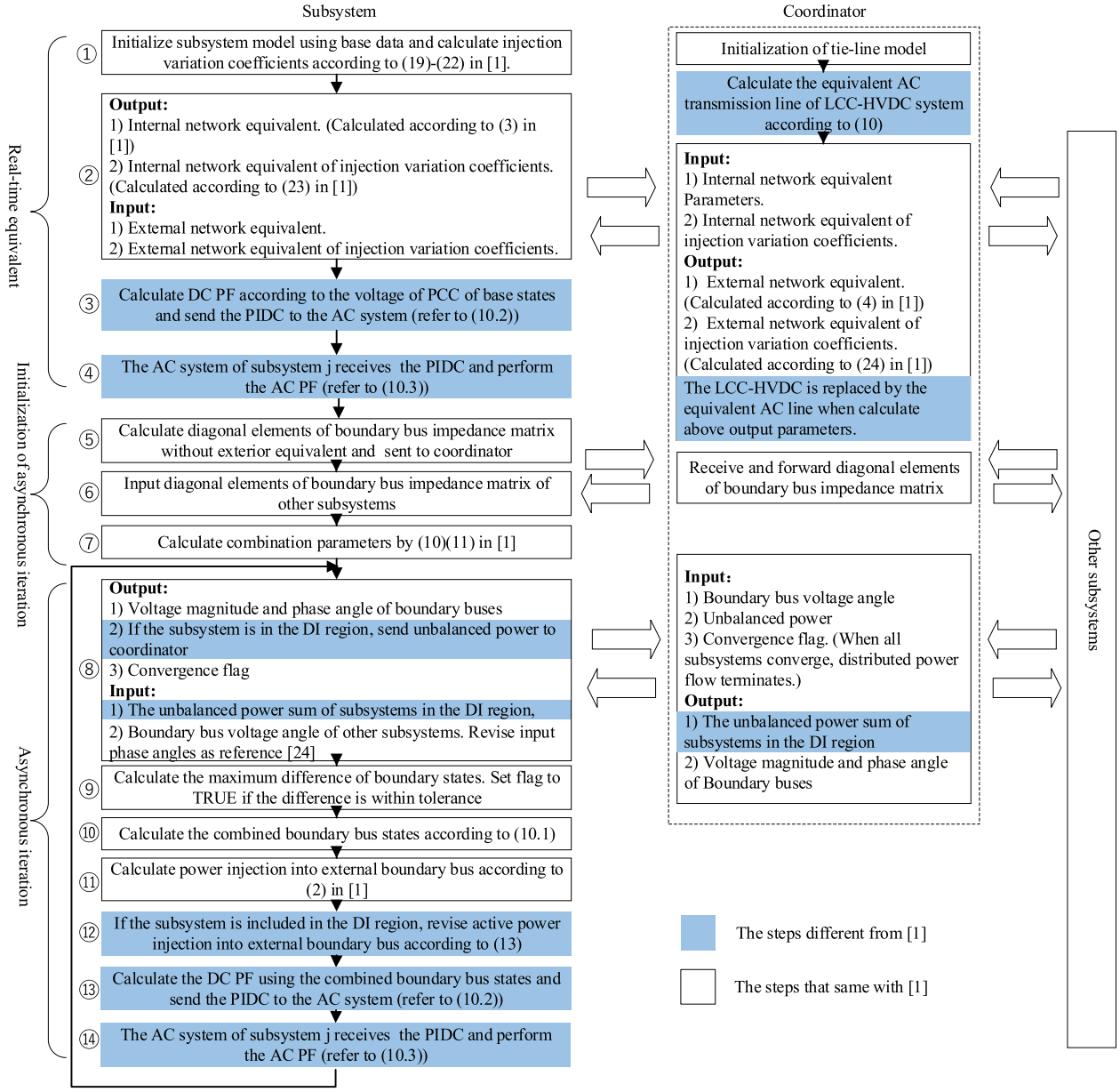

FIGURE 6. The flow chart of the algorithm.

bus states and the equivalent power injection into the external boundary buses. Besides, the subsystem in the DI region needs to correct the equivalent power injection to make the distribution of unbalanced power reasonable. Then, the DC PF is calculated according to the combined boundary bus states and the PIDC is obtained, also the control mode and the turns ratio of the converter transformer are adjusted. Finally, the AC PF is calculated according to the equivalent power injection into the external boundary buses and the PIDC, which generated the new boundary bus states for the next iteration.

Other different aspects should be noted. If the calculation of parameters involved in the algorithm is related to the DC system (such as combination parameters ξ_k, external network equivalent of injection variation coefficients μ_{BE_i}, etc.), the DC system should be replaced by its equivalent AC transmission line.

VI. THE CASE THAT THE DC SYSTEM IS MODELED IN THE COORDINATOR

In this paper, the DC tie-line model is built in the subsystem and the DC PF is carried out by the subsystem (defined as the preferred method). Considering there are some scenarios where the subsystem is not suitable for modeling the DC system, the DC tie-line can also be modeled and calculated in the coordinator (defined as the alternative method).

In this case, the process of fixed-point iteration is as follows. In the coordinator, the boundary bus states uploaded by each subsystem are combined according to (10.1), and the

combined boundary bus states are used to calculate DC PF according to (10.2). Then, the coordinator forwards the PIDC and the combined boundary bus states to relevant subsystems. After receiving the PIDC and the combined boundary bus states, the subsystem calculates the AC PF according to (10.3). When the AC PF calculation converges, the subsystem uploads the boundary bus states to the coordinator. The above process is repeated until the distributed calculation converges.

In fact, the above process is not fundamentally different from that of the preferred method, so it will not affect the results of the distributed calculation but will affect the amount of exchange data and the effect of asynchronous iteration. For the preferred method, the independence of the subsystem is stronger, the asynchronous iteration effect is better, and the amount of exchange data is small as each subsystem does not need to exchange the PIDC with the coordinator. For the alternative method, the asynchronous iteration effect is slightly poor, and the amount of data exchanged is increased, but the advantage is that the computing load of the subsystem is reduced.

In addition, the alternative method is more convenient for distributed calculation in the case of pure DC tie-line. As the DC system is regarded as the load at PCC in the AC PF, there is no electrical connection between the internal network and the external network when the subsystem calculates the AC PF. Therefore, the AC system of the subsystem only calculates the power flow of the internal AC network, and the PCC voltage required for the DC PF is given by the AC PF of each subsystem. The DC PF is carried out uniformly in the coordinator, so it is not necessary to consider the consistency of the calculation results of the DC system. When all tie-lines are DC line, the distributed calculation mode proposed in this paper will degenerate into the same calculation mode as described in [10].

VII. TEST RESULTS

A. MODIFIED IEEE 118-BUS SYSTEM

The algorithm was tested on the IEEE 118-bus system [25] with DC tie-lines added. The IEEE 118-bus system consists of 186 branches, 91 loads, and 54 generators. Branch {33(1)-15(2)}, {34(1)-19(2)}, {38(1)-30(2)}, {24(1)-23(2)}, {74(3)-70(1)}, {75(3)-70(1)}, {75(3)-69(1)}, {69(1)-77(3)} and {68(1)-81(3)} are taken as tie-lines (the number in brackets is the serial number of the subsystems). The IEEE 118-bus system is divided into three subsystems, and 30-38 and 81-68 are modified as DC lines. Define CEA as the constant control extinction angle, CIA as the constant control trigger angle, and CC as the constant control current. The control modes of the DC tie-lines are as follows:

DC line 30-38: the CC is 0.63 p.u. on the rectifier side, and the CEA is 17° on the inverter side.

DC line 81-68: the CC is 0.2 p.u. on the rectifier side, and the CEA is 17° on the inverter side.

In addition, the range of the trigger angle is set to $5° \sim 25°$, and the range of the extinction angle is set to $10° \sim 25°$. For the convenience of testing, we set the adjustment range of the tap position as ± 10. The initial turns ratio of each subsystem is set as 1.0. The disturbance in the test is set as follows: Bus 35 increases the 60 MW active load.

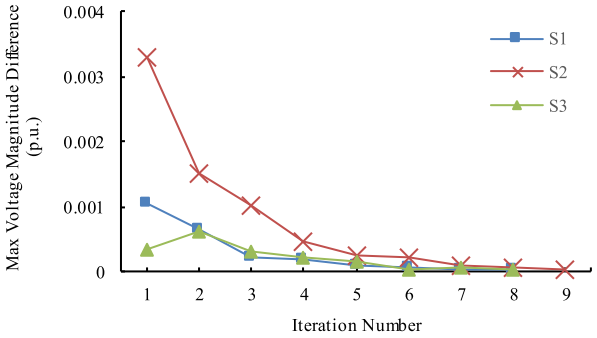

FIGURE 7. Maximum voltage magnitude difference compared with whole system power flow results.

To test the asynchronous iteration efficiency of the algorithm, each outer iteration selects 2 subsystems successively for the calculation.

The distributed algorithm and the centralized algorithm are used to calculate the power flow of the test system. Among them, the centralized algorithm adopts the sequential method mentioned in section II, and the unbalanced power caused by disturbance is also limited to be distributed in the DI region. The limit of bus voltage magnitude is set as 0.95 p.u. to 1.05 p.u., and all bus voltages are not out of limit in the following test results.

S1, S2, and S3 in Fig. 7 represent the three subsystems of the test system. Besides, the y-axis in Fig. 7 refers to the maximum voltage magnitude difference between distributed calculation and centralized calculation, and the x-axis refers to the number of the outer iteration. The voltage magnitude of distributed calculation is calculated in step ⑭ of the flow chart in Fig 6.

As can be seen from Fig. 7, with the progress of iteration, the error between the calculation results of each subsystem and the centralized calculation results decreases continuously, and all the subsystems finally get the power flow results consistent with the centralized calculation. The parameters of the equivalent AC line is calculated according to (10) in the real-time equivalent stage in Fig. 6. Following Table 1 shows the parameters of the equivalent AC line. "R" in brackets of DC tie lines 30(R)-38(I) and 81(R)-68(I) represents the rectifier side, while "I" in brackets represents the inverter side.

Also, Table 2 shows the base operation states of the DC tie-line. The base operation states data is a known condition to calculate the parameters in Table 1.

Table 3 compares the DC system calculation results of the distributed calculation and centralized calculation.

As can be seen from Table 3, after the disturbance occurs, the transformation ratio of the converter transformer obtained by the distributed calculation is completely consistent with the centralized calculation, which proves that the algorithm can correctly adjust the converter transformer's tap changer

TABLE 1. Parameters of the equivalent AC line.

DC tie-line	The parameters of the equivalent AC line (p.u.)			
	G_{DC}^{eq}	B_{DC}^{eq}	$b_{DC.R}^{eq}$	$b_{DC.I}^{eq}$
30(R)-38(I)	10.138	-39.329	1.059	-1.810
81(R)-68(I)	0.554	-7.233	-0.175	0.016

TABLE 2. Base operation states of the DC tie-line.

DC tie-line	The base operation states of DC tie-line (p.u.)						
	$P_{DC.R}$	$Q_{DC.R}$	$P_{DC.I}$	$Q_{DC.I}$	U_R	U_I	θ_{RI} (rad)
30(R)-38(I)	0.765	0.357	-0.749	0.305	0.990	0.951	0.010
81(R)-68(I)	0.257	0.079	-0.256	0.088	0.993	1.004	0.036

TABLE 3. Power flow calculation results of the DC system.

	Distributed computing		Centralized computing	
Bus	30/38	81/68	30/38	81/68
Active power	0.808973/ -0.793097	0.257494/ -0.256694	0.809010/ -0.793134	0.257494/ -0.256694
Reactive power	0.385721/ 0.310063	0.089025/ 0.084167	0.385622/ 0.310074	0.089025/ 0.084167
Transformer ratio	1.07/1.06	1.02/1.00	1.07/1.06	1.02/1.00
Control mode	CC0.63/ CEA17°	CC0.2/ CEA17°	CC0.63/ CEA17°	CC0.2/ CEA17°
Trigger angle	17.804209	17.861448	17.794636	17.861469

TABLE 4. Power flow calculation results of the DC system.

	Distributed computing		Centralized computing	
Bus	30/38	81/68	30/38	81/68
Active power	0.755360/ -0.742501	0.257489/ -0.256689	0.755119/ -0.742259	0.257492/ -0.256692
Reactive power	0.254466/ 0.183175	0.092245/ 0.087585	0.254424/ 0.186413	0.092237/ 0.087586
Transformer ratio	1.05/1.05	1.02/1.00	1.05/1.05	1.02/1.00
Control mode	CIA 5°/ CC0.57	CC0.2/ CEA17°	CIA 5°/ CC0.57	CC0.2/ CEA17°
Trigger angle	5.000000	17.845501	5.000000	17.843742

when the trigger angle or the extinction angle exceeds the limit. To test the processing effect of the algorithm on the control mode transformation, the upper limit of the converter transformer's turns ratio is set to 1.05, and the test is carried out again.

Table 4 shows that both distributed calculation and centralized calculation have transformed the control mode of the DC system, and the calculation results are consistent, which proves that the distributed algorithm can correctly handle the control mode transformation problem.

B. TEST OF A LARGE SYSTEM EXAMPLE

Artificially add tie-lines, interconnect the six IEEE 118-bus systems (defined as S1 to S6) together to build the test system, the serial number of bus is increased successively. Add the following transmission lines as tie-lines:

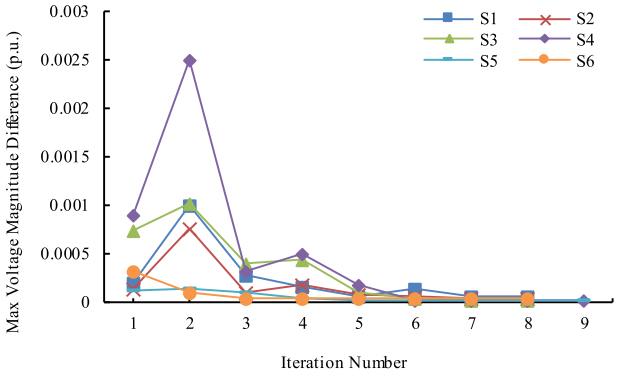

FIGURE 8. Maximum voltage magnitude difference compared with whole system power flow results.

{24(1)-141(2)}, {33(1)-133(2)}, {34(1)-137(2)}, {38(1)-148(2)}, {68(1)-317(3)}, {69(1)-313(3)}, {70(1)-310(3)}, {378(4)-495(5)}, {387(4)-487(5)}, {388(4)-491(5)}, {502(5)-392(4)}, {671(6)-422(4)}, {423(4)-667(6)}, {424(4)-664(6), {151(2)-249(3)}, {315(3)-433(4), {314(3)-432(4)}, {311(3)-429(4)}, and {505(5)-603(6)}.

In the above tie-lines, 671-422 and 317-68 are modified to DC lines, which adopt the control mode of constant control current on the rectifier and constant control extinction angle on the inverter. The disturbance set in the test is as follows: Bus 333 adds a 50 MW active load, and branch 91-92 are cut off. Each outer iteration selects 4 subsystems to participate in the calculation to test the asynchronous calculation of the algorithm.

Fig. 8 shows the maximum voltage magnitude error curve of the subsystems compared with that of the centralized calculation. It can be seen from the figure that the algorithm can still converge reliably when there are many subsystems.

Besides, we set different disturbances and tested the above case A and case B for 100 times. The method of disturbance setting is as follows. Firstly, a bus is randomly selected, and then an active load is added to the bus as a disturbance. The disturbance load values are randomly selected from 40MW, 80MW, and 120MW.

The tests are carried out in the same environment (Intel Core i5-7400 @3.00GHz, 8GB RAM). In Table 5, the average convergence number (the outer iteration number) and the average calculation time are given.

From Table 5, even if the overall scale and the number of subsystems of case B are much larger than those of case A, the convergence of the algorithm is not greatly affected, and the algorithm can still converge reliably. Therefore, the algorithm can well handle the distributed power flow calculation of AC/DC interconnected systems of various scales.

C. COMPARISON OF UNBALANCED POWER DISTRIBUTION METHOD

To compare the effect of the unbalanced power distribution method, the DC line of the test system in test case B is replaced by the AC line. The disturbance is as follows: bus 284 (Belong to S3) increases 180MW (about 1.8 p.u.)

TABLE 5. Convergence number and calculation time of different test cases.

	Test case A	Test case B
Average iteration number	4.515	6.816
Average calculation time	0.776s	2.804s

TABLE 6. Comparison of unbalanced power distribution method.

Subsystem	Unbalanced power of subsystem (p.u.)	
	The algorithm of [1]	The algorithm of this paper
S1	0.320172	0.447273
S2	0.298710	0.441426
S3	0.299564	0.465803
S4	0.297207	0.455718
S5	0.328986	-0.009747
S6	0.290699	0.004255

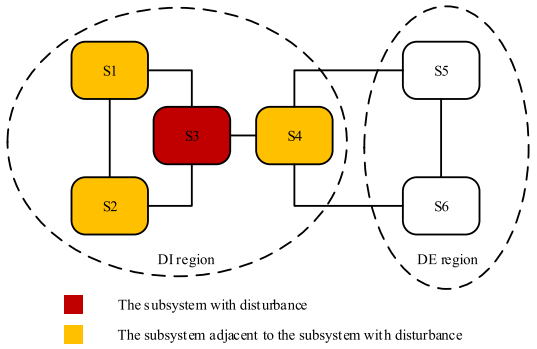

FIGURE 9. Schematic diagram of the test system.

active load. Other condition settings are consistent with test case B. The schematic diagram of the test system is shown below. The DI region and the DE region are also marked in the figure below.

According to the unbalanced power distribution method in this paper, the unbalanced power is distributed between the subsystems in the DI region, namely S1 to S4. According to reference [1], the unbalanced power is distributed between S1 to S6. The two algorithms are tested and compared. Taking $\Delta P'_{BE.SYSj}$ (related to step ⑫ in the flow chart Fig. 6) as y-axis and outer iteration number of subsystems as x-axis, the following two figures can be obtained respectively. Also, Table 6 shows the unbalanced power distribution results of the two algorithms.

According to Table 6, the unbalanced power distribution method achieved the expected effect. The power shortage caused by the disturbance (about 1.8 p.u.) is balanced by the subsystems in the DI region, and the subsystems in the DE region adjust the generator output according to the variation of transmission loss. The unbalanced power distribution method of this paper limited the influence of the disturbance in the DI region. However, In the algorithm of [1], the disturbance's influence spread to all subsystems, which is not in line with the actual situation.

From Fig. 10 and Fig. 11, the convergence of the new method is better than that of the old method. In Fig. 11, S5 and S6 may lead to overcorrection of unbalanced power, and this

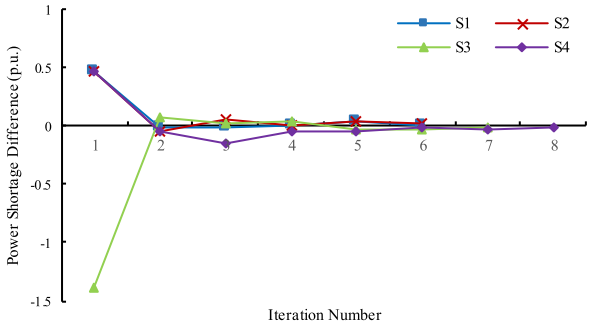

FIGURE 10. Correction value of boundary bus unbalanced power of the algorithm in this paper.

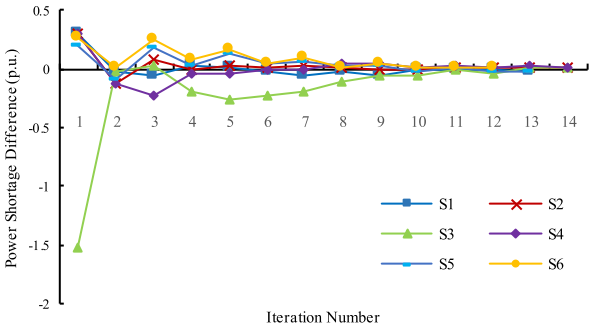

FIGURE 11. Correction value of boundary bus unbalanced power of the algorithm in [1].

error will be transmitted to other subsystems, and lead to poor convergence of the distributed calculation. Also, the fewer number of subsystems participating in unbalanced power distribution is a reason for the improvement of convergence.

VIII. CONCLUSION

The distributed AC/DC power flow algorithm proposed in this paper is obtained from the effective combination of the sequential method and the algorithm in reference [1]. Therefore, the algorithm retains the advantages of the algorithm in [1]. This paper presents some innovative methods to solve the problems in the implementation of the algorithm. For the problem of equivalent calculation of external network including DC line, the method of converting the DC line to the equivalent AC line is proposed. Also, to solve the problem that the discrete variables of the DC system are not easy to coordinate, a new fixed-point iteration scheme is constructed. In the new fixed-point iteration scheme, the combined PCC voltage is used to calculate the DC PF, which avoids the combination calculation of discrete variables. Besides, the paper improved the unbalanced power distribution method. The improvement is not only more in line with the practical situation, but also can get a better convergence than [1]. As shown in the test cases. when the network size and the number of subsystems increases, the convergence rate changes little. Moreover, since the power flow calculation of the AC/VSC-HVDC network can also use the sequential method, the proposed algorithm has the potential to be extended to the case of VSC-HVDC.

REFERENCES

[1] H. Zhang, B. Zhang, A. Bose, and H. Sun, "A distributed multi-control-center dynamic power flow algorithm based on asynchronous iteration scheme," *IEEE Trans. Power Syst.*, vol. 33, no. 2, pp. 1716–1724, Mar. 2018.

[2] M. Wolter, H. Guercke, T. Isermann, and L. Hofmann, "Multi-agent based distributed power flow calculation," in *Proc. IEEE PES Gen. Meeting*, Jul. 2010, pp. 1–6.

[3] B. H. Kim and R. Baldick, "A comparison of distributed optimal power flow algorithms," *IEEE Trans. Power Syst.*, vol. 15, no. 2, pp. 599–604, May 2000.

[4] T. Erseghe, "Distributed optimal power flow using ADMM," *IEEE Trans. Power Syst.*, vol. 29, no. 5, pp. 2370–2380, Sep. 2014.

[5] A. Engelmann, Y. Jiang, T. Muhlpfordt, B. Houska, and T. Faulwasser, "Toward distributed OPF using ALADIN," *IEEE Trans. Power Syst.*, vol. 34, no. 1, pp. 584–594, Jan. 2019.

[6] G. N. Korres, "A distributed multiarea state estimation," *IEEE Trans. Power Syst.*, vol. 26, no. 1, pp. 73–84, Feb. 2011.

[7] V. Kekatos and G. B. Giannakis, "Distributed robust power system state estimation," *IEEE Trans. Power Syst.*, vol. 28, no. 2, pp. 1617–1626, May 2013.

[8] L. Ao, B. Cheng, and F. Li, "Research of power flow parallel computing based on MPI and P-Q decomposition method," in *Proc. Int. Conf. Electr. Control Eng.*, Jun. 2010, pp. 2925–2928.

[9] D. Wang, F. Zhou, and J. Li, "Cloud-based parallel power flow calculation using resilient distributed datasets and directed acyclic graph," *J. Modern Power Syst. Clean Energy*, vol. 7, no. 1, pp. 65–77, Jan. 2019.

[10] J. Liu, X. Feng, B. Berggren, I. Segerqvist, and M. Callavik, "Distributed power flow analysis for hybrid AC/HVDC grids by network decomposition," in *Proc. IEEE PES Gen. Meeting |Conf. Expo.*, Jul. 2014, pp. 1–5.

[11] V. Donde, X. Feng, I. Segerqvist, and M. Callavik, "Distributed state estimation of hybrid AC/HVDC grids by network decomposition," *IEEE Trans. Smart Grid*, vol. 7, no. 2, pp. 974–981, Mar. 2016.

[12] N. Xia, H. B. Gooi, S. Chen, and W. Hu, "Decentralized state estimation for hybrid AC/DC microgrids," *IEEE Syst. J.*, vol. 12, no. 1, pp. 434–443, Mar. 2018.

[13] X. Kong, Z. Yan, R. Guo, X. Xu, and C. Fang, "Three-stage distributed state estimation for AC-DC hybrid distribution network under mixed measurement environment," *IEEE Access*, vol. 6, pp. 39027–39036, 2018.

[14] S. D. Manshadi and M. Khodayar, "Decentralized operation framework for hybrid AC/DC microgrid," in *Proc. North Amer. Power Symp. (NAPS)*, Sep. 2016, pp. 1–6.

[15] C. Qi, K. Wang, Y. Fu, G. Li, B. Han, R. Huang, and T. Pu, "A decentralized optimal operation of AC/DC hybrid distribution grids," *IEEE Trans. Smart Grid*, vol. 9, no. 6, pp. 6095–6105, Nov. 2018.

[16] Z. Liang, S. Lin, and M. Liu, "Distributed optimal power flow of AC/DC interconnected power grid using synchronous ADMM," in *Proc. IOP Conf. Ser., Mater. Sci. Eng.*, May 2017, pp. 12–13.

[17] D. A. Braunagel, L. A. Kraft, and J. L. Whysong, "Inclusion of DC converter and transmission equations directly in a Newton power flow," *IEEE Trans. Power App. Syst.*, vol. PAS-95, no. 1, pp. 76–88, Jan. 1976.

[18] J. Reeve, G. Fahny, and B. Stott, "Versatile load flow method for multiterminal HVDC systems," *IEEE Trans. Power App. Syst.*, vol. PAS-96, no. 3, pp. 925–933, May 1977.

[19] P. Kundur, *Power System Stability and Control*. New York, NY, USA: McGrawHill, 1994, p. 545.

[20] R. Ramanathan, H. Ramchandani, and S. A. Sackett, "Dynamic load flow technique for power system simulators," *IEEE Trans. Power Syst.*, vol. 1, no. 3, pp. 25–30, Aug. 1986.

[21] J. Meisel, "System incremental cost calculations using the participation factor load-flow formulation," *IEEE Trans. Power Syst.*, vol. 8, no. 1, pp. 357–363, Feb. 1993.

[22] B. Stott and O. Alsac, "Fast decoupled load flow," *IEEE Trans. Power App. Syst.*, vol. PAS-93, no. 3, pp. 859–869, May 1974.

[23] K. L. Lo, L. J. Peng, J. F. Macqueen, A. O. Ekwue, and N. H. Dandachi, "Extended Ward equivalent of external system for on-line security analysis," in *Proc. 2nd Int. Conf. Adv. Power Syst. Control, Operation Manage., APSCOM*, Hong Kong, Dec. 1993, pp. 54–59.

[24] G. M. Huang and J. Lei, "A concurrent non-recursive textured algorithm for distributed multi-utility state estimation," in *Proc. IEEE Power Eng. Soc. Summer Meeting*, Jul. 2002, pp. 1570–1575.

[25] A. R. Al-Roomi. (2015). *Power Flow Test Systems Repository*. [Online]. Available: https://al-roomi.org/power-flow/118-bus-system

HAIBO ZHANG (Senior Member, IEEE) was born in Heilongjiang, China, in 1975. He received the Ph.D. degree from the Department of Electrical Engineering, Tsinghua University, Beijing, China, in 2005. He is currently a Professor with North China Electric Power University, Beijing. His research interests include energy management system (EMS) and new energy power system planning, operation, and control.

SHUAI WANG was born in Hunan, China, in 1996. He is currently pursuing the master's degree with North China Electric Power University, Beijing, China. His research interest includes distributed power flow.